Ore Geology Reviews 131 (2021) 104041

Contents lists available at ScienceDirect

Ore Geology Reviews

journal homepage: www.elsevier.com/locate/oregeorev

Generation and structural modification of the giant Kengdenongshe VMS-type Au-Ag-Pb-Zn polymetallic deposit in the East Kunlun Orogen, East Tethys: Constraints from geology, fluid inclusions, noble gas and stable isotopes

Xu Zhao [a,b], Lebing Fu [b,*], Junhao Wei [b], Jan M Huizenga [c,d], Yan Liu [b], Jiajie Chen [e], Dianzhong Wang [f]

[a] CAS Key Laboratory of Mineralogy and Metallogeny/Guangdong Provincial Key Laboratory of Mineral Physics and Materials, Guangzhou Institute of Geochemistry, Chinese Academy of Sciences, Guangzhou 510640, China
[b] School of Earth Resources, China University of Geosciences, Wuhan 430074, China
[c] Economic Geology Research Institute (EGRU), College of Science and Engineering, James Cook University, Townsville 4811, Queensland, Australia
[d] Department of Geology, University of Johannesburg, PO 524, Auckland Park, 2006, South Africa
[e] School of Earth Science, East China University of Technology, Nanchang 330013, China
[f] State Key Laboratory of Ore Deposit Geochemistry, Institute of Geochemistry, Chinese Academy of Sciences, Guiyang 550081, China

ARTICLE INFO

Keywords:
Polymetallic deposit
Fluid inclusions
Stable isotope
Noble gas isotope
East Kunlun Orogen
VMS

ABSTRACT

The Kengdenongshe giant Au-Ag-Pb-Zn polymetallic deposit is located in the East Kunlun Orogen (EKO). It contains about 42.2 t of Au, 608.6 t of Ag and 1.05 Mt of Pb and Zn with an average grade of Au 2.31 g/t, Ag 19.29 g/t and Pb + Zn 3.49 wt% (Pb: 1.23 wt%, Zn: 2.26 wt%). The NWW-trending ore bodies are predominantly hosted in Late Permian to Triassic rhyolitic tuff, which formed during Late Permian back-arc extension to Triassic arc-continental collision. The ore bodies are subdivided into Pb-Zn rich ore bodies on the top with high grades of Pb and Zn and low grades of Au and Ag, and Au-Ag rich ore bodies below with high grades of Au and Ag and low grades of Pb and Zn. The Pb-Zn rich ore bodies occur as vein, stockwork, and in breccia, and comprise quartz, pyrite, galena, sphalerite, and small amounts of chalcopyrite. The Au-Ag rich ore bodies consist of auriferous barite-sulfide-oxide veins and contain barite, pyrite (early strawberry and oolitic pyrite and later eu- to subhedral pyrite), galena, sphalerite, chalcopyrite, tetrahedrite and covellite. Gold is present as electrum, kustelite and native gold and silver is present as polybasite, pearceite, kongsbergite, and as minor native silver in microfractures in sulfides. The hydrothermal alteration minerals include, from bottom to top, quartz + barite + calcite around the Au-Ag rich orebodies, quartz + chlorite + epidote around the Pb-Zn rich orebodies, and quartz + K-feldspar within the tuff. Fluid inclusions from both the Pb-Zn rich and the Au-Ag rich orebodies consist of two phases (V–L-type) fluid inclusions of which the vapor phase has a size of 10–40 vol%. Fluid inclusions microthermometry reveal homogenization temperatures of fluid inclusions in Pb-Zn rich and Au-Ag rich ore bodies of 128–230 °C and 110–320 °C, with corresponding salinities of 0.7–9.9 and 0.2–18.3 wt% NaCl equivalent, respectively. H-O-S-Pb stable isotope and He-Ar noble gas isotope data indicate a mixed magmatic water-seawater source for both the Pb-Zn and Au-Ag rich ore bodies, and an additional meteoric water component for the Au-Ag rich ore bodies. The Pb-Zn and Au-Ag rich ore bodies share the same sulfur and lead sources, i.e. sulfur is derived from crustal magma and seawater/marine sulfate, and the lead originated from a mixed magmatic-ancient crustal sedimentary source. Collectively, the regional geology, mineralogy, alteration, and geochemistry indicate that the Kengdenongshe Au-Ag-Pb-Zn polymetallic deposit can be characterized as a VMS-type (volcanic-associated massive sulfide) deposit. Formation of the ore-hosting rhyolite tuff and mineralization are associated with Late Permian to Triassic marine volcanic exhalation. Middle to Late Triassic basin closure and arc-continent collision modified the deposit and resulted in the location inversion of the Pb-Zn and Au-Ag rich orebodies.

* Corresponding author.
E-mail address: fulb@cug.edu.cn (L. Fu).

https://doi.org/10.1016/j.oregeorev.2021.104041
Received 26 November 2020; Received in revised form 20 January 2021; Accepted 26 January 2021
Available online 2 February 2021

1. Introduction

The East Kunlun Orogen (EKO) records the evolutionary history of the Tethys Ocean during which it generated extensive metal ore deposits (Xiong et al., 2014; Zhang et al., 2005; Ma et al., 2015; Chen et al., 2016, 2017; Zhao et al., 2018). The Kengdenongshe giant Au-Ag-Pb-Zn polymetallic deposit is located in the east end of the EKO and contains large amounts of Pb-Zn and Au-Ag in the same space, which is representative and distinguished from the predominant Au only or Pb-Zn only deposits in the region. The orebodies in the Kengdenongshe are hosted in Late Permian to Triassic rhyolitic tuff comprising ca. 42.2 t of Au, 608.6 t of Ag and 1.05 Mt of Pb and Zn with average grade of Au 2.31 g/t, Ag 19.29 g/t and Pb + Zn 3.49 wt% (Pb: 1.23 wt%, Zn: 2.26 wt%). The original stratigraphic relationships, structure, and mineral assemblage of the Kengdenongshe polymetallic deposit is obscured by later tectonic dislocation (Liu et al., 2018), and the generation and structural modification processes of it are still unclear.

Late Permian to Early Triassic back-arc extension is recently defined in the Kengdenongshe area (Zhao et al., 2019, 2020), which supports the Kengdenongshe deposit possibly to be Au-Ag related VMS (volcanic-associated massive sulfide) deposit, as the Au-Ag related VMS deposits are generally associated with an extensional setting, i.e. in rifted settings within arcs and back-arcs (Barrie and Hannington, 1999; Gibson et al., 2000; McNicoll et al., 2008; Mercier-Langevin et al., 2011) and associated with felsic volcanic rocks (Huston, 2000; Allen et al., 2002; Lafrance et al., 2005; Herrington et al., 2005; Chiaradia et al., 2008; Mills et al., 2016). Previous studies have proposed different origins of Au-Ag in Au-related VMS deposits. Mercier-Langevin et al (2007) suggested that the early to *syn*-volcanic introduction of Au-Ag and Pb-Zn in the LaRonde Penna gold-rich VMS from the Abitibi greenstone belt is supported by mine sequence stratigraphy, but later deformation and alteration may have been responsible for the introduction of Au in other world-class gold-rich VMS deposits. Previous studies have suggested that the accumulation of Pb-Zn and Au may not have occurred at the same time (Herzig and Hannington, 1995; Emsbo et al., 1999., Tomkins, 2007), as Pb-Zn mostly migrated as chloride complexes and precipitated under conditions of increased sulfur concentration in fluids, while Au usually precipitated in an opposite scenario. The orebodies of the Kengdenongshe polymetallic deposit can be subdivided into Au-Ag rich and Pb-Zn rich orebodies. The Au-Ag rich orebodies usually coexist with barite and are located below the Pb-Zn rich orebodies. The genetic relationship of the Au-Ag rich orebodies and Pb-Zn rich orebodies is also unclear, i.e. the introduction of Au-Ag-Pb-Zn in this deposit needs to be further constrained.

In this paper, we provide regional geological, fluid inclusions, and H-O-S-Pb-He-Ar isotope data to constrain the formation and modification of the Kengdenongshe polymetallic deposit and we determine the genetic relationship between the Au-Ag rich and the Pb-Zn rich orebodies in this deposit.

2. Geological setting

2.1. Geology of the East Kunlun Orogen

The EKO, composing of the northern part of the Tibetan plateau, is separated from Qaidam Basin by the North Eastern Kunlun Suture Zone (NEKS) in the north and from the West Kunlun Orogen by the Altyn fault belt in the west. It is bounded to south by the Bayan Har terrane and adjacent to the Qinling orogenic belt to east (Fig. 1a; Xu and Li., 2006; Xu et al, 2015; Zhao et al., 2018). The EKO is subdivided into the Northern East Kunlun Terrane and the Southern East Kunlun Terrane, which are separated by the Central East Kunlun Suture Zone (CEKS) and Southern East Kunlun Suture Zone (SEKS) (Fig. 1b). These two famous regional sutures, the CEKS and SEKS, traversing the EKO, are considered to result from closures of the Proto-Tethys Ocean in the Middle Devonian and the Paleo-Tethys Ocean in the Middle Triassic, respectively (Ma et al., 2015., Zhao et al., 2018). The initial subduction of the Proto-Tethys Ocean in the EKO started in Late Cambrian and closed in Early Silurian (Yang et al., 1996; Liu et al., 2011; Zhang et al., 2014), accompanied by Middle to Late Ordovician back-arc extension (Gao et al., 2010). The initial subduction of the Paleo-Tethys Ocean was earlier than Early Permian and the back-arc extension occurred during the Late Permian to Early Triassic (Chen et al., 2004; Zhao et al., 2019). Final basin closure and continental collision occurred in the Middle Triassic (Chen et al., 2017; Chen, 2018). The oldest units in the EKO include the amphibolite-facies metamorphic rocks of the Paleoproterozoic Jinshuikou Group (Chen et al., 2006; Wang et al., 2007) and Mesoproterozoic to Neoproterozoic Xiaomiao Formation (Wang et al., 2004; Jin et al., 2015; He et al., 2016). These rocks are overlain by the Ordovician Naij Tai Group (Chen et al., 2013) comprising low-grade *meta*-volcanic and *meta*-sedimentary rocks, and discontinuous Carboniferous to Neogene sedimentary and volcanic rocks (Chen et al., 2017, Fig. 1b). Ordovician-Devonian (470–390 Ma) and Permian-Triassic (260–220 Ma) calc-alkaline granodiorites, monzogranites, and

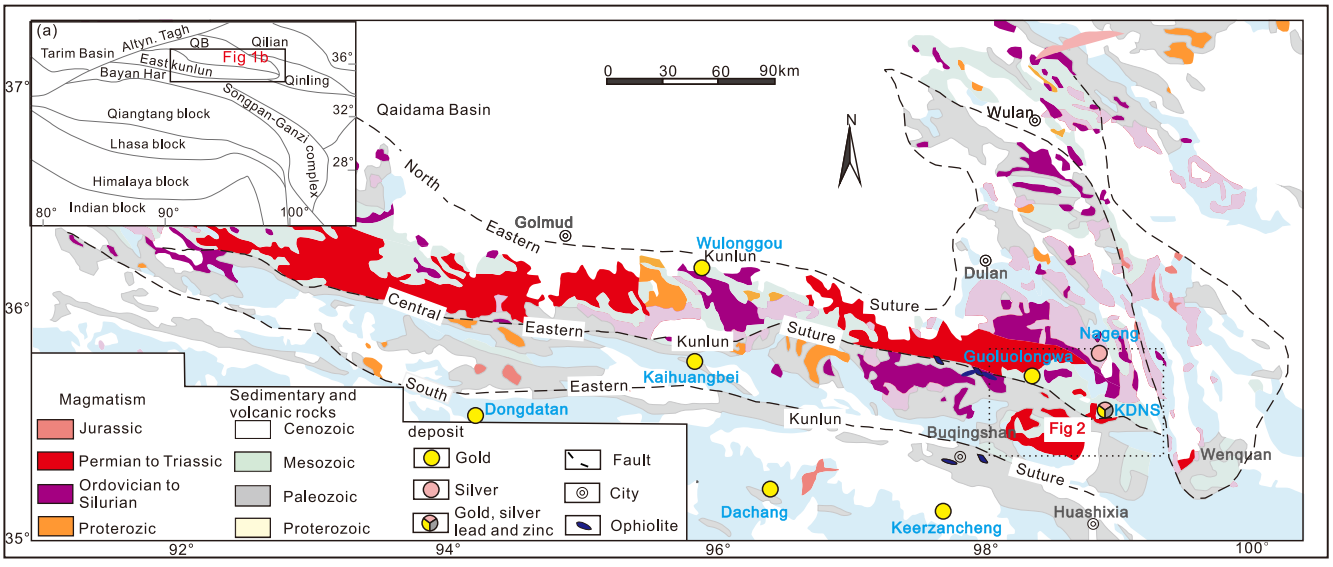

Fig.1. Simplified geological map of: (a) the Qinghai-Tibetan Plateau showing the dominated terranes. (b) the Eastern Kunlun Orogen showing the location of study area. QB: Qaidama Basin.

syenogranites are widespread in the EKO (Mo et al., 2007; Chen, 2018).

2.2. Geology of the Gouli orefield

The Gouli study area is situated in the eastern part of the EKO (Fig. 1b). NWW-trending structures, including the CEKS, control the regional distribution of the sedimentary and magmatic rocks (Fig. 2). The NWW-trending structures, together with small-scale NNE-trending structures, control the directions of ore bodies in the Gouli ore field. Proterozoic medium to high grade metamorphic basement rocks occur across the entire area. The basement rocks are covered by Ordovician to Silurian *meta*-volcanic and *meta*-sedimentary rocks, Carboniferous sedimentary rocks, and Permian to Triassic sedimentary and volcanic rocks. These rocks are intruded by widely distributed Permian to Triassic arc granitoids, and Late Triassic *syn*-collision and post-collision granitic rocks (Chen et al., 2017), and locally occurring mafic rocks (Zhao et al., 2019, 2020; Fig. 2). Previous studies on the Late Permian to Middle Triassic intrusions in this area suggested that the tectonic setting of the EKO evolved from Late Permian to Early Triassic back-arc basin through Early to Middle Triassic ongoing oceanic subduction to Middle Triassic continental collision (Chen et al., 2017; Chen, 2018; Zhao et al., 2020).

Several large to middle-sized metal deposits have been discovered in the Gouli ore field, including the Guoluolongwa Au (>40 t Au), Annage Au (>8 t Au), Asiha Au (>6 t Au), Walega Au (>12 t Au), Delong Au (>5 t Au), Nageng Ag (>2000 t Ag), and the Kengdenongshe polymetallic deposits (Fig. 2). The Kengdenongshe Au-Ag-Pb-Zn polymetallic deposit is the only one of its kind in the region.

3. Geology, mineralization and alteration of the Kengdenongshe polymetallic deposit

3.1. Geology of the Kengdenongshe polymetallic deposit

The Kengdenongshe polymetallic deposit is located in the north of the CEKS (Fig. 2) and hosted in Late Permian to Triassic rhyolitic tuff. The tuff is grey to green in color and comprises subhedral quartz (25–30 vol%), plagioclase (10–15 vol%), K-feldspar grains (5–10 vol%), and minor felsic fragments (40–45 vol%) with little barite, zircon, titanite, and Fe-Ti oxides. Quartz, plagioclase, and K-feldspar usually form subhedral and are<2 mm in length. Rhyolitic tuff in the near vicinity of the ore bodies contain sericite, chlorite, and carbonate, and increased contents of Fe oxides and barite. Previous studies demonstrate that the tuff was derived from the crustal reworking and related to the tectonic transition from Late Permian back-arc extension to Middle Triassic arc-continent collision (Zhao et al., 2020).

In the south the rhyolitic tuff is in tectonic contact with limestone and marble from the Carboniferous Haoteluowa Formation, and in the north the rhyolitic tuff is in tectonic contact with schist and gneiss from the Paleoproterozoic Jinshuikou Group (Fig. 3). These tectonic contacts are defined by ~ 20 m wide W-NW trending reverse faults dipping 30-65° to the SW (Fig. 3). Gabbro (266 Ma) intruded in the north of the mining area (Fig. 2; Zhao et al., 2019) and locally occurring granite porphyry intruded in the gneiss and rhyolitic tuff at 257 and 211 Ma, respectively (Fig. 3; Zhao et al., 2020). The gabbro and granite porphyries indicate the initiation of Late Permian back-arc extension in the Kengdenongshe area (Zhao et al., 2019, 2020).

3.2. Mineralization and alteration

Twenty-two NW-trending polymetallic ore bodies have been explored in the Kengdenongshe district and can be further subdivided into two types due to different metal grades, mineral assemblage and alteration. The type 1 ore bodies are Pb-Zn rich ore bodies. There are thirteen type 1 ore bodies with relatively high average grades of Pb (0.90 wt%) and Zn (2.77 wt%), and relatively low average grades of Au (0.20 g/t), and Ag (5.65 g/t). They often occur as lodes and bands within the tuff and the mineralized zones commonly dip 50°-85° to the NNE-NE (Fig. 4). They extend for 80 to 560 m, are 1 to 32 m thick, and continue up to 850 m down plunge. The other nine ore bodies are dominated by Au and Ag and have relatively high average grades of Au (3.67 g/t) and

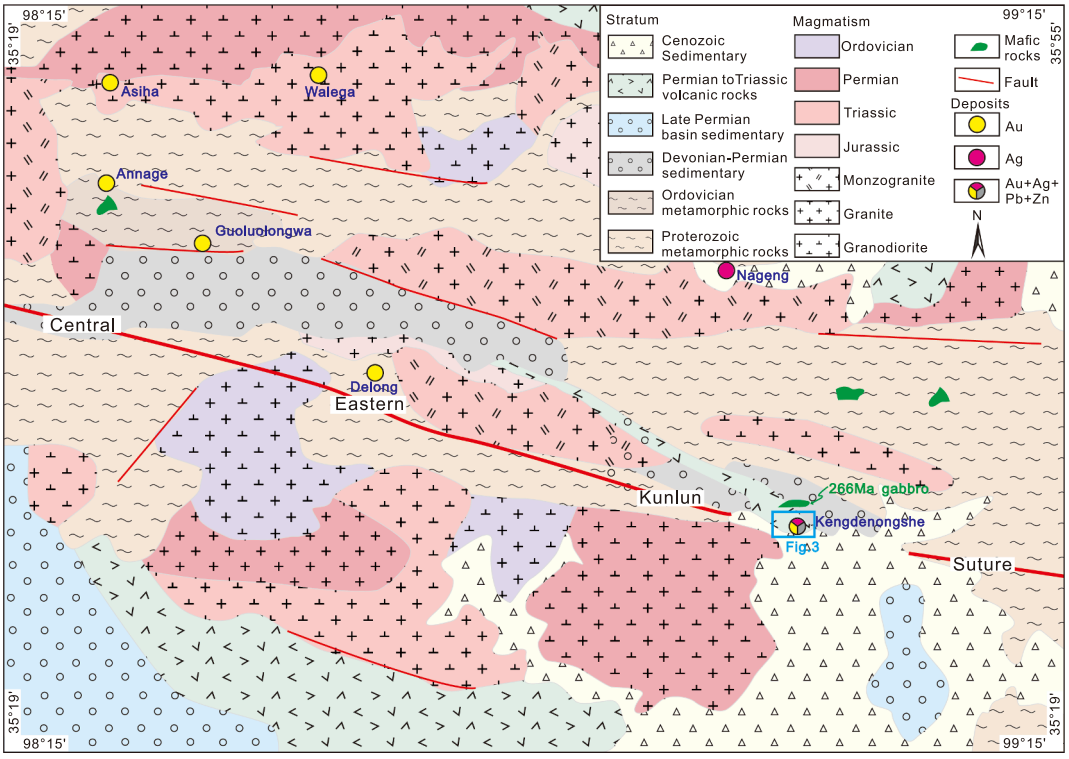

Fig.2. Geological map of the Gouli field showing the location of Kengdenongshe polymetallic deposit, the ages of the gabbro in north of the Kengdenongshe is from Zhao et al. (2019).

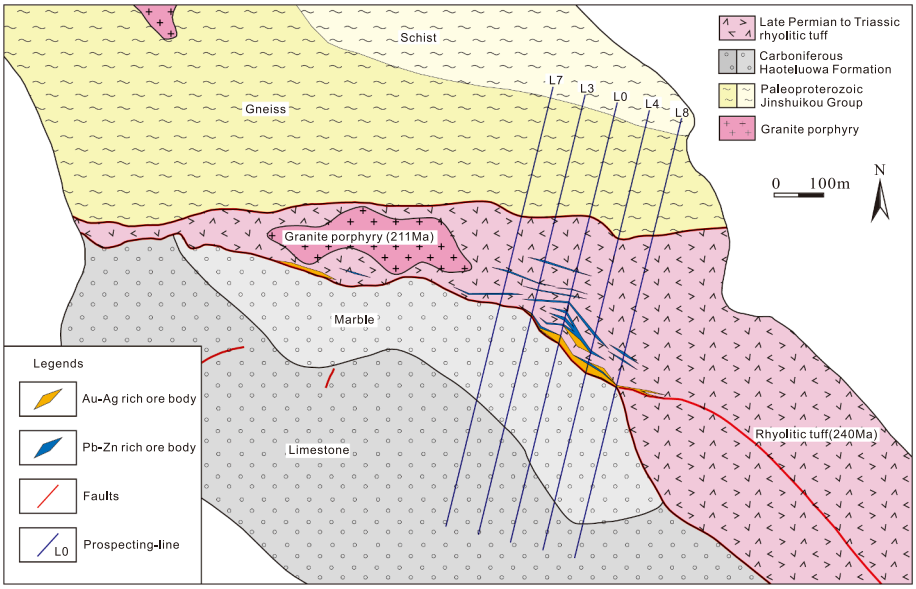

Fig. 3. Simplified geological map of the Kengdenongshe area showing the location of the ore bodies.

Ag (52.78 g/t), and relatively low average grades of Pb (0.52%) and Zn (0.65%) (type 2: Au-Ag rich ore bodies), which usually occur near or at the tuff-carbonatite contact area (Fig. 4). They are controlled by NW-trending faults and usually have forms of lodes and lensoids with mineralized zones commonly trending 15°–30° and dipping 65°–85°. Single veins of the Au-Ag rich ore bodies are 2 to 43 m thick, extend for 40 to 800 m, and continue up to 800 m down plunge (Fig. 4).

The Pb-Zn rich ore bodies mainly consist of quartz, pyrite, galena, sphalerite, and chalcopyrite (Fig. 5). Euhedral to subhedral pyrites are usually included by the sphalerite or galena (Fig. 5i, k), and sometimes display breccia structure (Fig. 5j). Small amounts of chalcopyrite grow within the sphalerite or in the fractures between the pyrite grains (Fig. 5h, j), and small calcite veins occasionally intersect in the Pb-Zn sulfides (Fig. 5l). The Pb-Zn orebodies have been deformed by later structural activity as evidenced by the fractured Lead-zinc mineralized tuffs in the fault zones (Fig. 5a).

The Au-Ag rich orebodies contain barite, pyrite, galena, sphalerite, chalcopyrite, and minor amounts tetrahedrite and covellite (Fig. 6). The pyrites are subdivided into two types. The first pyrite type is strawberry or oolitic pyrite with a diameter of<0.1 mm (Py1, Fig. 6h, j-l). These pyrites typically show micro-fractures filled with chalcopyrite, tetrahedrite, and barite (Fig. 6j). The second pyrite type is eu- to subhedral with a diameter up to 5 mm (Py2, Fig. 6j, i). Type 2 pyrite and other sulfides including galena, sphalerite and chalcopyrite usually occur around type 1 pyrite (Fig. 6j), indicating that the formation of the eu- to subhedral type 2 pyrite and other sulfides is later than the strawberry or oolitic type 1 pyrite. Veins comprising type 2 pyrite contain tuff breccia (Fig. 6e), indicating that its formation is associated with the tectonic event that deformed the tuff and ore bodies. Gold is present as electrum, kustelite and native gold and silver is present as polybasite, pearceite, and minor native silver and kongsbergite in the microfractures of these sulfides (Guo et al., 2013; Li et al., 2016).

Hydrothermal alteration minerals in the Kengdenongshe polymetallic deposit include (from bottom to top) quartz + barite + calcite, quartz + chlorite + epidote, and quartz + K-feldspar (Figs. 7 and 8). The alteration zone around the Au-Ag rich orebodies comprises quartz + barite + calcite and has a minimum width of several centimeters up to one meter (Figs. 7 and 8). Quartz + chlorite + epidote alteration (width of several tens of meters) is widespread around the Pb-Zn rich orebodies (Fig. 7). The alteration of quartz + K-feldspar occurs within the tuff outcrop and sometimes has a scale of several meters (Fig. 8).

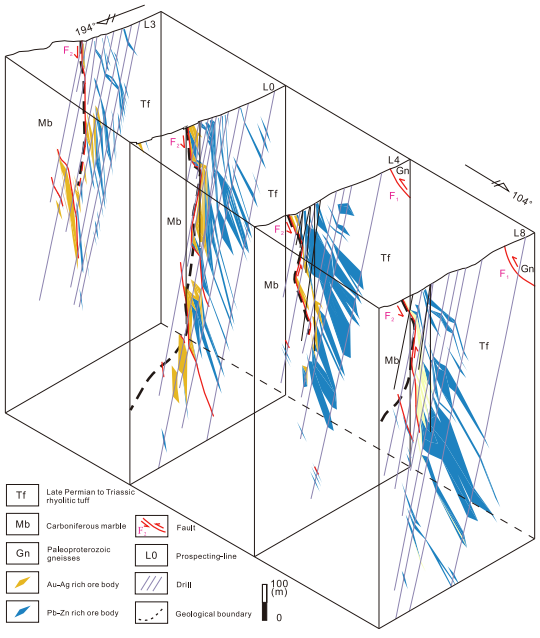

Fig. 4. Combined profiles of the major prospecting lines in the Kengdenongshe polymetallic deposit, the locations of these prospecting lines are shown in Fig. 3.

4. Analytical methods

4.1. Fluid inclusion microthermometry

Microthermometric measurements of fluid inclusions were performed at the State Key Laboratory of Geological Processes and Mineral Resources (GPMR), China University of Geosciences (CUG), using a Linkam THM600 heating-freezing stage attached to a Leica MD2500 microscope. The estimated accuracy was ± 0.1 °C for the final melting temperature of ice and ± 2 °C for homogenization temperatures. Homogenization always occurred into the liquid phase. Salinities of two-phases fluid inclusions expressed as wt.% NaCl equivalent were calculated using the MacFlincor software (Brown and Hagemann, 1995).

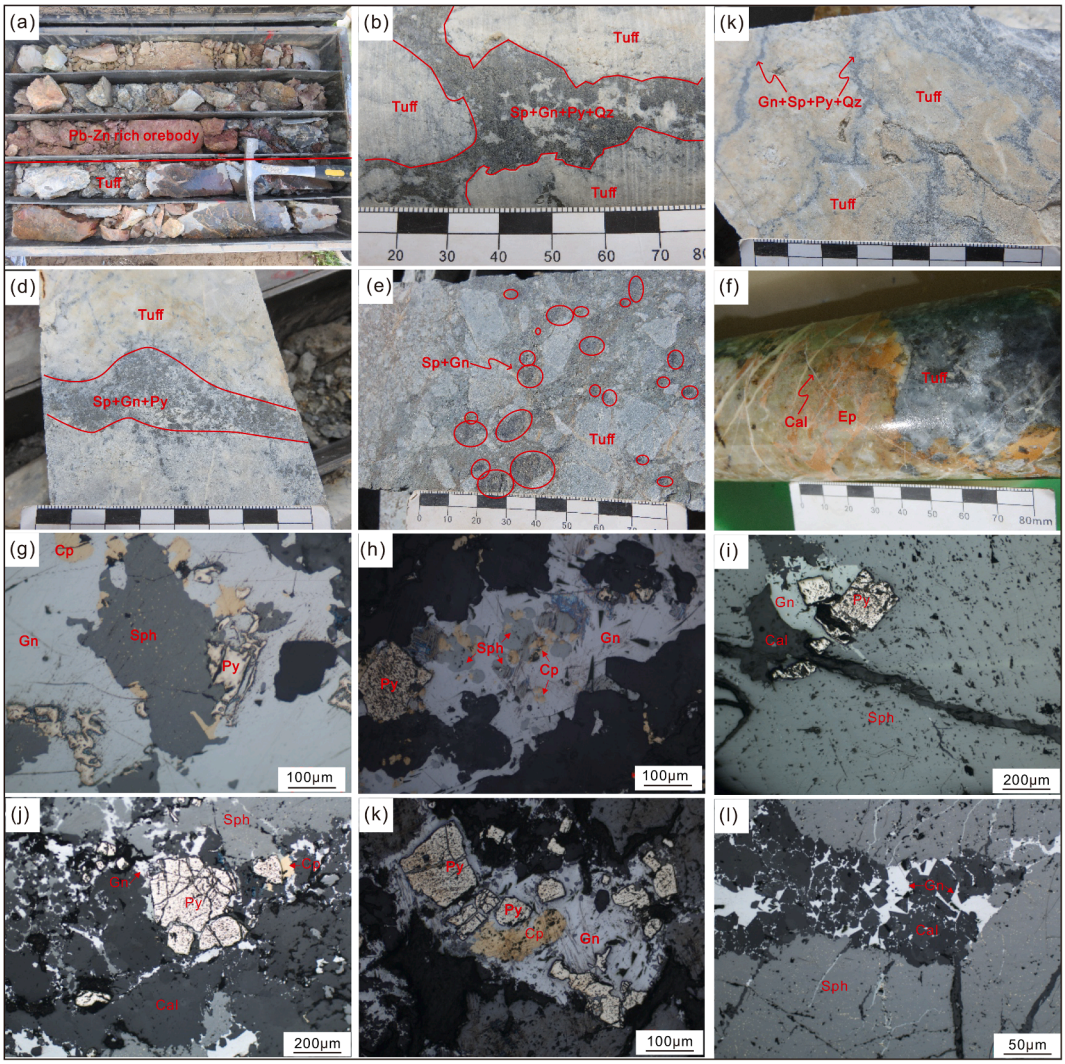

Fig. 5. The field and microscopic photographs from the Pb-Zn rich ore bodies in the Kengdenongshe polymetallic deposit. Cal: calcite; Cp: chalcopyrite; Gn: galena; Sph: sphalerite; Py: pyrite.

4.2. H-O stable isotope analyses

The H-O stable isotopic analyses were performed at the Beijing Research Institute of Uranium Geology (BRIUG) using a MAT-253 mass spectrometer. Quartz and barite samples for H-O isotopic analyses were hand-picked and separated using a magnetic separator. Oxygen was liberated from samples by reaction with BrF_5 (Clayton and Mayeda, 1963) and converted to CO_2 on a platinum-coated carbon rod. Analyses of the hydrogen isotopic compositions of fluid inclusions were done on the same samples that were used for oxygen isotope analysis. Samples were first degassed of labile volatiles by heating under vacuum at 150 °C for 3 h. Water was released by heating the samples to approximately 500 °C using an induction furnace and converted to hydrogen by passage over heated zinc powder at 410 °C. The $\delta^{18}O$ and δD determinations were made on a MAT-253 stable isotope ratio mass spectrometer. The analytical precision was better than ± 0.2‰ for $\delta^{18}O$ and ± 2‰ for δD.

4.3. S-Pb stable isotope analyses

The S-Pb stable isotope analyses were also performed at the BRIUG using a MAT-253 mass spectrometer. All minerals used for analyses were handpicked and checked under a binocular microscope to ensure purity of > 98%. Sulfur isotopic ratios were measured on a Delta V plus mass spectrometer, using the VCDT standard. The analytical error is lesser than ± 0.2‰. Lead isotope analyses were performed by using a thermal ionization mass spectrometry (ISOPROBE-T). The error of measured Pb isotopic ratio of the international standard NBS981 is around 0.1‰.

4.4. He-Ar isotope analyses

Pyrite samples for noble gas isotopic analysis were crushed and sieved to pass the 20–40 mesh fractions. Helium and argon isotope compositions were measured on an MI-1201IG inert gas mass spectrometer at the Institute of Geology and Geophysics, Chinese Academic of Sciences. Noble gases were extracted from the mineral grains by crushing in a one-step or multi-step process in a vacuum crusher at 2000 psi. The Ar in the noble gas mixtures was trapped in a cold finger with charcoal at the temperature of liquid nitrogen. Helium was trapped in a cold finger at about 13 K and released at 35 K. He and Ar were introduced separately into the mass spectrometer and analyzed in static mode. Line blanks were run before samples. He blanks were negligible ($^3He < 3 \times 10^{-17}$ cc STP); and Ar blanks were low ($^{40}Ar < 4 \times 10^{-11}$ cc STP), about 0.1% of the signal from samples. The data were corrected for system blank and further calibrated by air shot and Helium HESJ standards (He Standard of Japan; Matsuda et al., 2002). The recommended value of the $^3He/^4He$ ratio of HESJ relative to the air value (R/Ra) is 20.63 ± 0.10. $^{40}Ar/^{36}Ar$ ratios are accurate to ± 1% and $^3He/^4He$ ratios are within ± 5% over the range 10^{-6}-10^{-8} cm^3 STP ^4He.

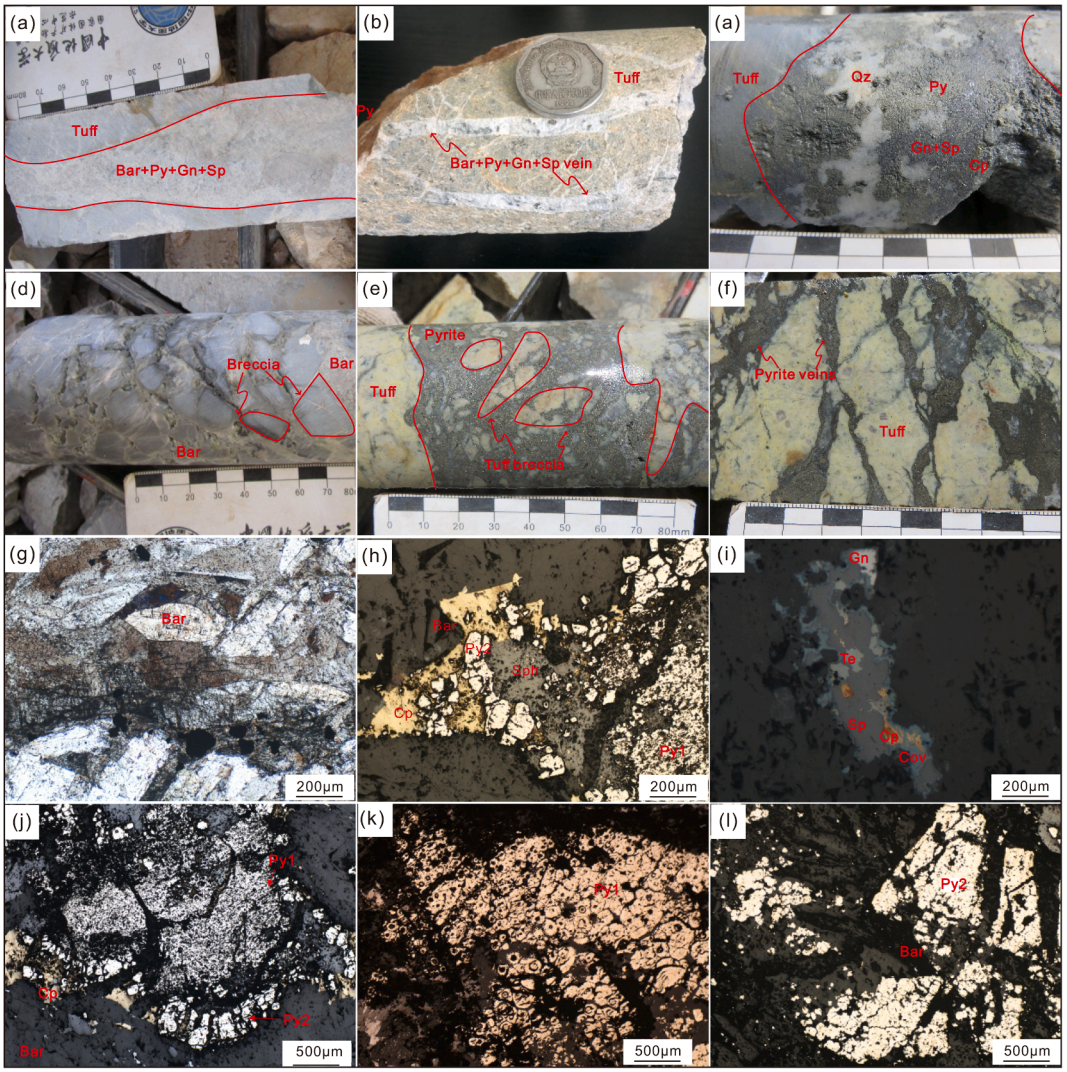

Fig. 6. The field and microscopic photographs from the Au-Ag rich ore bodies in the Kengdenongshe polymetallic deposit. Cp: chalcopyrite; Gn: galena; Sph: sphalerite; Py: pyrite; Te: tetrahedrite; Cov: covellite.

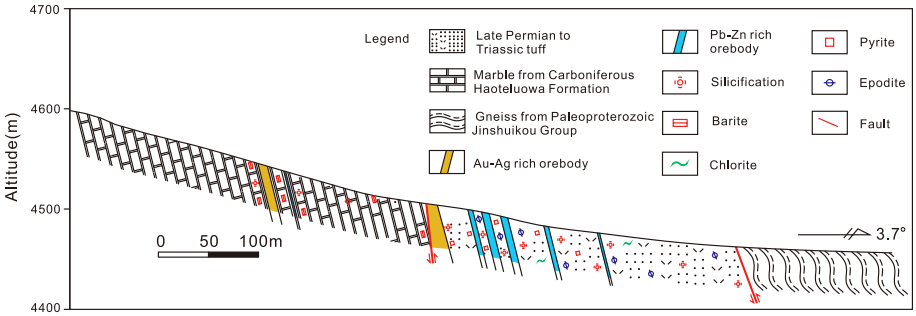

Fig. 7. Profile map of the L0 in Fig. 3 showing the alterations around Au-Ag and Pb-Zn rich ore bodies.

5. Results

5.1. Microthermometric measurements of fluid inclusion

Aqueous isolated liquid–vapour fluid inclusions (vapour phase: 10–40 vol%) in the quartz from Pb-Zn rich orebodies are < 10 um in size and show a rounded or negative crystal shapes (Fig. 9a, b). Liquid-vapor fluid inclusions (<10 um, volume of the vapour phase: 5–45 vol%) in quartz and barite from the Au-Ag rich ore bodies consist of two phases (V–L-type) (Fig. 9c, d) and show irregular and rounded shapes.

The microthermometric characteristics of the fluid inclusions from different ore bodies described below and the associated data are summarized in Table 1 and Fig. 10. The temperatures of the final ice melting for the V–L-type fluid inclusions from the Pb-Zn rich and Au-Ag rich ore bodies range from − 1.0 to − 6.7 °C and − 0.2 to − 6.8 °C, and the corresponding salinities are 0.7–9.9 wt% NaCl equivalent and 0.2–18.3 wt% NaCl equivalent, respectively. The homogenization temperatures for the fluid inclusions in Pb-Zn rich orebodies range between 128 and 223 °C, peaking at 150–170 °C, and those in the Au-Ag rich orebodies range between 110 and 320 °C, peaking at 130 °C to 170 °C.

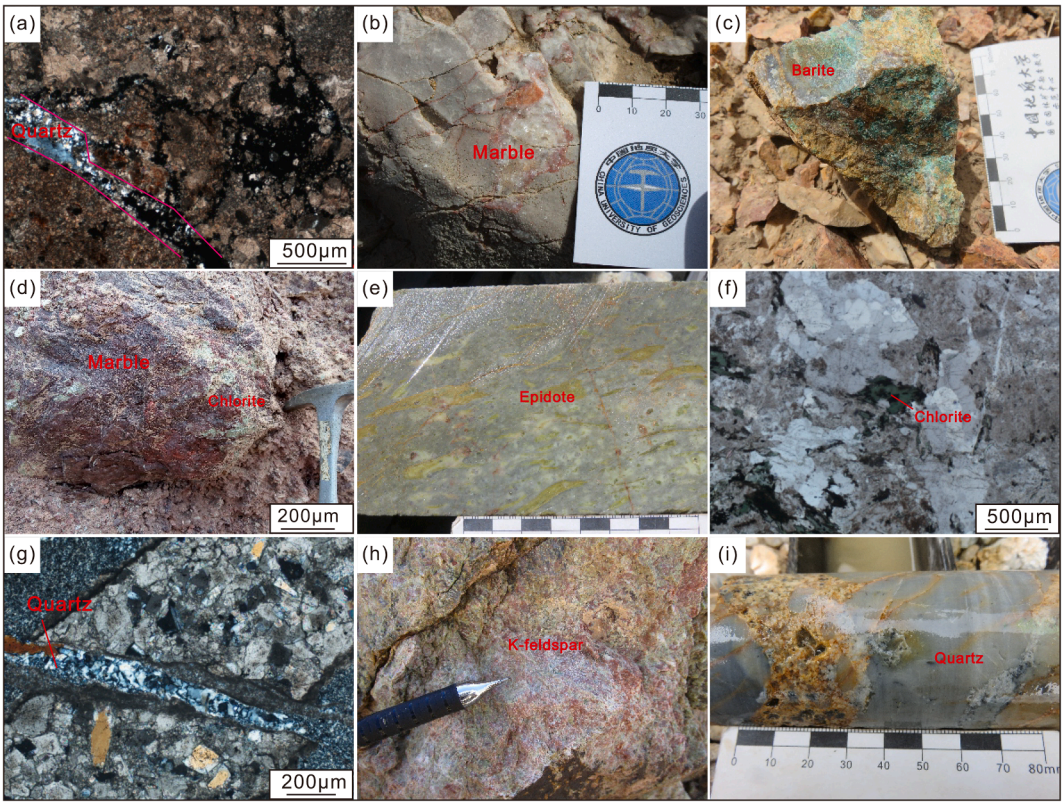

Fig. 8. The field and microscopic photographs for the hydrothermal alteration minerals. (a–c) from the Au-Ag rich orebodies, (d–g) from the Pb-Zn rich orebodies and (h–i) from the rhyolitic tuff outcrop.

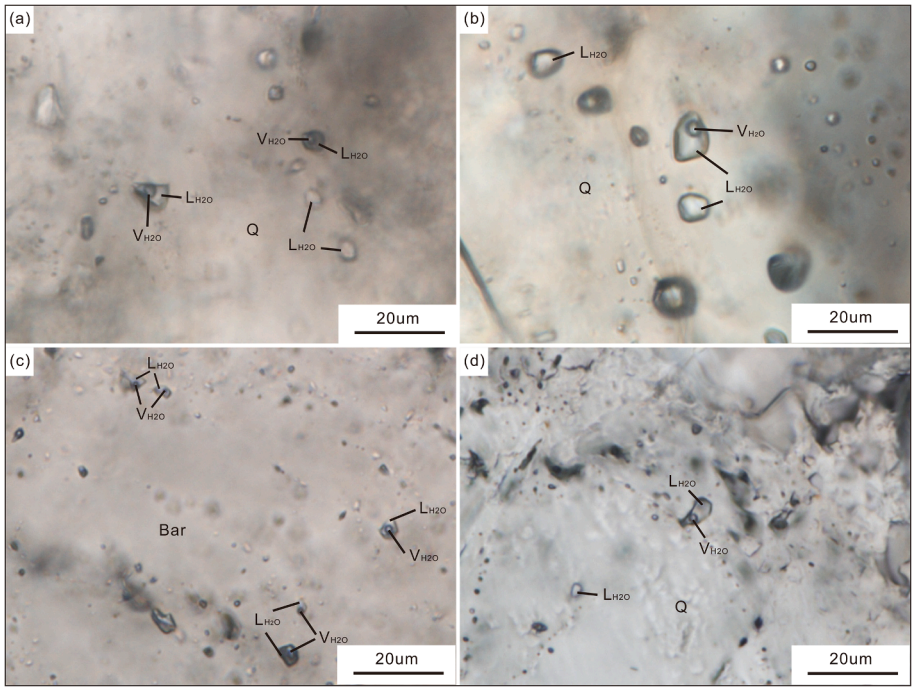

Fig. 9. Microscopic photographs for fluid inclusions from Pb-Zn rich orebodies (a-b) and Au-Ag rich orebodies (c-d). Q: quartz; Bar: barite.

5.2. H–O isotopes

Hydrogen and oxygen isotopic data are displayed in Table 2 and Fig. 11. Hydrogen and oxygen of fluid inclusions in quartz from Pb-Zn rich ore bodies have measured δD values of –91.6 to –93.0‰, $\delta^{18}O$ values of 11.0 to 12.4‰ and calculated $\delta^{18}O_{H2O}$ values in equilibrium with quartz of 2.6 to 4.0‰. The measured δD and $\delta_{18}O$ values for barite in Au-Ag rich ore bodies display ranges from –75.1 to –109.6‰ and 8.8 to 17.4‰, respectively (Table 2). The calculated $\delta^{18}O_{H2O}$ values of the ore-forming fluids in equilibrium with barite range from 0.8 to 9.4‰.

Table 1
Microthermometric fluid inclusion data for Pb-Zn and Au-Ag rich ore bodies in the Kengdenongshe polymetallic deposit.

Sample No	Ore bodies	Type	Host mineral	Number	Vapor (vol. %)	Th (°C)	Salinity (wt.% NaCl)	Reference
B3302-2–4	Pb-Zn rich	L.V	Quartz	33	10–40	128–223	1.7–9.9	This paper
ZK0009-19	Pb-Zn rich	L.V	Quartz	15	15–55	165–230	0.7–3.6	Jiang, 2014
B3302-8–1	Au-Ag rich	L.V	Quartz	21	5–40	110–262	0.7–14.5	This paper
B3302-5–2	Au-Ag rich	L.V	Barite	15	5–45	150–320	4.2–18.3	This paper
ZK0007-07	Au-Ag rich	L.V	Barite	16	10–55	142–331	0.2–4.4	Jiang, 2014
ZK0007-18	Au-Ag rich	L.V	Barite	15	10–40	126–330	0.2–11.0	Jiang, 2014
ZK0007-19	Au-Ag rich	L.V	Barite	15	15–30	105–254	0.2–11.3	Jiang, 2014

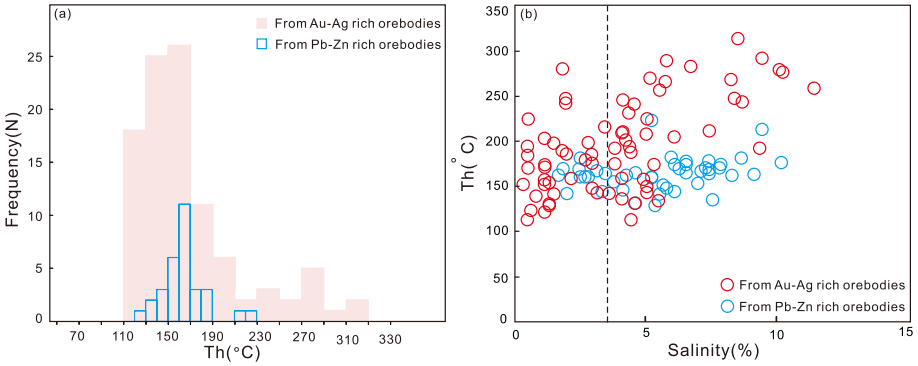

Fig. 10. (a) Homogenization temperature histograms and (b) Homogenization temperature versus salinity plots for fluid inclusions from different ore bodies.

5.3. S-Pb isotopes

In the sulfides from the Pb-Zn rich ore bodies, the $\delta^{34}S$ values for pyrite are from −3.3 to 2.9‰, for galena are from 4.7‰ to 7.1‰ (Table 3 and Fig. 12). As to the sulfides and barite from the Au-Ag rich ore bodies, the $\delta^{34}S$ value for pyrite is −3.5‰, and for barites is 28.3‰.

The Pb isotope ratios for galena and pyrite are relatively homogeneous with $(^{206}Pb/^{204}Pb)_i$ = 18.297–18.363, $(^{207}Pb/^{204}Pb)_i$ = 15.577–15.668 and $(^{208}Pb/^{204}Pb)_i$ = 38.193–38.490 from Pb-Zn rich ore bodies and $(^{206}Pb/^{204}Pb)_i$ = 18.300–18.389, $(^{207}Pb/^{204}Pb)_i$ = 15.584–15.570 and $(^{208}Pb/^{204}Pb)_i$ = 38.221–38.591 from Au-Ag rich ore bodies. These values are different from the Pb isotope compositions of the tuff with $(^{206}Pb/^{204}Pb)_i$ = 17.545–18.177, $(^{207}Pb/^{204}Pb)_i$ = 15.546–15.634 and $(^{208}Pb/^{204}Pb)_i$ = 37.993–38.975 (Table 4, Fig. 13).

5.4. He–Ar isotope

Noble gas (He and Ar) isotope compositions measured for pyrite are listed in Table 5 and illustrated in Fig. 14. The obtained $^3He/^4He$ ratios of fluid inclusions in the pyrite from Pb-Zn rich ore bodies and Au-Ag rich ore bodies are 0.02–0.06 Ra and 0.06–0.07 Ra, respectively. The $^{40}Ar/^{36}Ar$ ratios are 297.0–1011.7 in the pyrite-hosted fluid inclusions from the Pb-Zn rich ore bodies and 318.2–347.5 in the pyrite-hosted

Table 2
Hydrogen and oxygen isotopic compositions of the barite and quartz from Pb-Zn and Au-Ag rich ore bodies in the Kengdenongshe polymetallic deposit.

Sample No	Ore bodies	Mineral	δD_{H2O}/‰	$\delta O_{V\text{-}SMOW}$/‰	δO_{H2O}/‰
B3302-4–4	Pb-Zn rich	Quartz	−93.0	12.4	4.0
B0008-2–3	Pb-Zn rich	Quartz	−92.7	11.0	2.6
B0808-26–4	Pb-Zn rich	Quartz	−91.6	11.4	3.0
B3501-1	Au-Ag rich	Barite	−81.1	10.4	2.4
B3302-8–1	Au-Ag rich	Barite	−95.6	9.4	1.4
B0806-29–1	Au-Ag rich	Barite	−101.3	8.8	0.8
B3302-5–2	Au-Ag rich	Barite	−109.6	10.4	2.4
B3302-5–3	Au-Ag rich	Barite	−97.3	10.4	2.4
B0303-6–1	Au-Ag rich	Barite	−75.1	17.4	9.4

The Calculation formulas for the δO_{H2O} are from Clayton et al (1972)

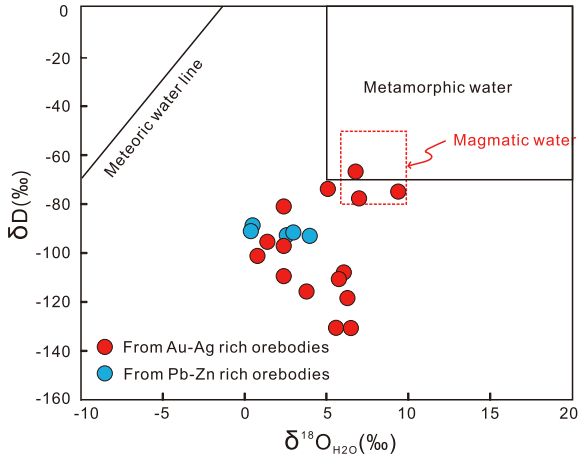

Fig. 11. The δD–$\delta^{18}O_{H2O}$ plots for mineralizing fluids from the Kengdenongshe polymetallic deposit. Part of the data is cited from He (2013) and Jiang (2014). The meteoric water line is from Chen and Wang. (2004). The ranges of primary magmatic and metamorphic water are from Misra (2000).

Table 3
Sulfur isotopic compositions of the barite and sulfides from Pb-Zn and Au-Ag rich ore bodies in the Kengdenongshe polymetallic deposit.

Sample No	Ore bodies	Mineral	$\delta^{34}S_{V\text{-}CTD}$(‰)
B0806-26–3	Pb-Zn rich	Pyrite	−3.3
B0812-1	Pb-Zn rich	Pyrite	2.9
B0809-1	Pb-Zn rich	Pyrite	−3.0
B0810-1	Pb-Zn rich	Pyrite	1.5
B0809-1	Pb-Zn rich	Galena	4.9
B0808-5–5	Pb-Zn rich	Galena	4.7
B0006-2–5	Pb-Zn rich	Galena	6.7
B0008-4–6	Pb-Zn rich	Galena	7.1
B3501-1	Au-Ag rich	Barite	28.3
B3501-1	Au-Ag rich	Pyrite	−3.5

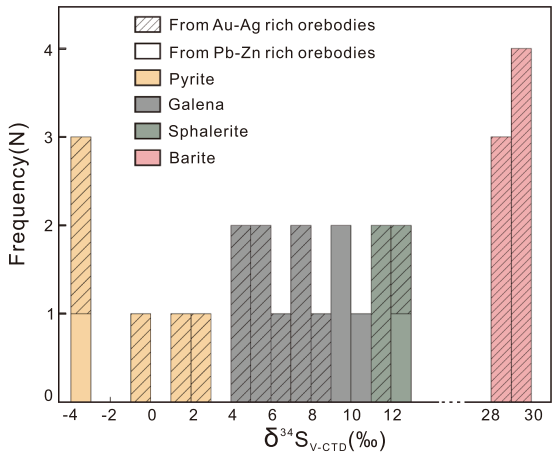

Fig. 12. The sulfur isotope compositions of sulphides and barite from the Kengdenongshe polymetallic deposit. Part of the data is from Jiang (2014).

fluid inclusions from the Au-Ag rich ore bodies.

6. Discussion

6.1. Constraints on fluid source and fluid evolution

The δD and δ_{18} O_{H2O} values in both Pb-Zn-rich and Au-Ag-rich orebodies are lower than those in magmatic fluids and plot between the magmatic fluids and seawater/meteoric water (Fig. 11), which means the fluids may derive from the mixing of magmatic water and seawater/meteoric water (Ouyang et al., 2014; Ke et al., 2017). The $^3He/^4He$ ratios of fluid inclusions extracted from pyrites in Pb-Zn rich ore bodies (0.01–0.07 Ra) exhibit similar values to those attributed to seawater (0.01–0.05 Ra, Fig. 14, Stuart et al., 1995; Ozima and Podosek, 2002), indicating that the main mixing source for the fluid in Pb-Zn rich orebodies should be seawater. The higher $^3He/^4He$ ratios from Au-Ag rich orebodies than those from Pb-Zn rich orebodies may suggest the extra contribution of meteoric water for Au-Ag rich orebodies, as meteoric water usually show higher $^3He/^4He$ ratios than seawater (Mamyrin and Tolstikhin, 1984). Although air-derived noble gas is likely to be presented, its effect is minor in comparison to the large range $^{40}Ar/^{36}Ar$ ratios (Fig. 14), which should be attributed to the hydrothermal fluids associated with magmatism (Burnard et al., 1999; Tang et al., 2017).

The homogenization temperatures (110–310 °C), δD values (–131 to –74) and $\delta^{18}O_{H2O}$ (0.8–9.4) values for fluid inclusions from Au-Ag rich orebodies are more variable than those from Pb-Zn rich orebodies, (homogenization temperatures: 128–223 °C; δD = –88.7 to –93.0; $\delta^{18}O_{H2O}$ = 0.4–3.0). This suggests different mixing sources and processes (Fig. 10a), which is also indicated by the distinct homogenization temperature vs. salinity trends (Fig. 10b). The simple mixing of a high temperature, high salinity magmatic fluid and a low temperature, low salinity meteoric water can result in the decrease of both homogenization temperatures and salinities, which is consistent with the fluid inclusion data of the Au-Ag rich ore bodies (Fig. 10b). However, with regard to the Pb-Zn rich ore bodies, the homogenization temperatures remain stable while the salinity is variable. This could result from the mixing of cooler magmatic water and heated seawater. If heat conduction between the hot magmatic fluid and cold seawater occurred before fluid mixing, the cooled magmatic water and heated seawater will have the same temperature but show different salinities. Subsequent mixing of the magmatic fluid and the seawater would result in a stable fluid temperature but variable salinities (Hou et al., 2001; Liu et al., 2018).

6.2. Source of sulfur and metals

The forms of sulfur in a hydrothermal system could be sulfide (S^{2-}), sulfate (SO_4^{2-}), sulfur dioxide (SO_2) and hydrogen sulfide (H_2S) depending on temperature, PH and oxygen fugacity. Ohmoto (1972) summarized the relationship between the chemical environment in hydrothermal systems and the sulfur isotope composition of hydrothermal minerals as follows. (1) In higher oxygen fugacity at low pH conditions, the sulfur mainly presents in sulfates, and the $\delta^{34}S$ values in barite are about equal to or slightly larger than total $\delta^{34}S$ values in fluids ($\delta^{34}S_{\sum S}$). (2) In moderate oxygen fugacity and high pH conditions, sulfides and sulfates coexist and the $\delta^{34}S_{\sum S}$ values are between the $\delta^{34}S$ values in barite and sulfides. (3) At low oxygen fugacity conditions, barite is usually insoluble in water, and the possible mineral combinations are sulfides of pyrite + pyrrhotite + galena + sphalerite. The values of $\delta^{34}S$ in these sulfides are equivalent to the $\delta^{34}S_{\sum S}$ (Ohmoto, 1972; Ohmoto and Rye, 1979).

The barites in the Au-Ag rich orebodies precipitated from a hydrothermal fluid, which is evidenced by occurrence of primary inclusions in the barites (Fig. 9c). These barites coexist with sulfides, and the barite $\delta^{34}S$ values are much higher than the $\delta^{34}S$ sulphide values ($\delta^{34}S$ = –4‰ to + 12‰, average value is + 6‰) (Fig. 12). This suggests that the barite and sulfides precipitated at a moderate oxygen fugacity and high pH conditions, and that the $\delta^{34}S_{\sum S}$ values were between the values from barites (+28 to + 30 ‰) and sulfides (–4 to + 12 ‰). As discussed above, magmatic fluids with a crustal source play an important role in generating the Au-Ag rich orebodies. However, in a crust-derived magmatic fluid, the $\delta^{34}S$ values are less likely to be higher than + 12‰ and show no wide range. Thus, the high $\delta^{34}S$ values suggest the contamination with seawater sulfur ($\delta^{34}S \approx +20‰$) (e.g. Anderson et al., 1998; Basuki et al., 2008; Dixon and Davidson, 1996), which is also supported by the contribution of seawater to ore-forming fluids. As for the Pb-Zn rich orebodies, the sulfides have similar $\delta^{34}S$ values as the sulfides from the Au-Ag rich orebodies (Fig. 12), suggesting that the Pb-Zn rich orebodies may have the same sulfur source, i.e. a mixed magma-seawater source.

The same lead source for the Pb-Zn rich orebodies and Au-Ag rich orebodies is indicated by the same linear variations of the lead isotopic compositions of the sulfides (Fig. 13a, b). The plots of the sulfides on $^{206}Pb/^{204}Pb$ vs $^{207}Pb/^{204}Pb$ and $^{206}Pb/^{204}Pb$ vs $^{208}Pb/^{204}Pb$ diagrams only partially overlap with the Late Permian to Triassic magmatic rocks, suggesting that Triassic magmatism cannot be the only lead source. Possible contamination of old crustal sedimentary rocks is indicated by the partial overlap of the lead isotope ratios between the sulfide and

Table 4
Lead isotopic compositions of the sulfides, tuff and granite porphyry in the Kengdenongshe polymetallic deposit.

Samples No	Sulfide/rocks	$^{206}Pb/^{204}Pb$	$^{207}Pb/^{204}Pb$	$^{208}Pb/^{204}Pb$
B0810-1	Pyrite from Pb-Zn rich orebody	18.357	15.657	38.458
B0812-1	Pyrite from Pb-Zn rich orebody	18.303	15.613	38.306
B0809-1	Pyrite from Pb-Zn rich orebody	18.363	15.668	38.490
B0809-2	Galena from Pb-Zn rich orebody	18.297	15.577	38.193
B3309-1	Pyrite from Au-Ag rich orebody	18.389	15.698	38.591
B3309-2	Galena from Au-Ag rich orebody	18.300	15.584	38.221
B0806-0–1	Tuff	18.177	15.570	38.975
B0806-4–1	Tuff	17.545	15.546	37.993
B0806-29–3	Tuff	17.747	15.592	38.367
B0808-5–6	Tuff	17.588	15.551	38.047
80303–11-1	Tuff	17.613	15.634	38.302
B0008-1–2	granite porphyry	17.569	15.588	38.107
B0008-1–3	granite porphyry	17.581	15.579	38.108
B0008-1–4	granite porphyry	18.052	15.590	38.738

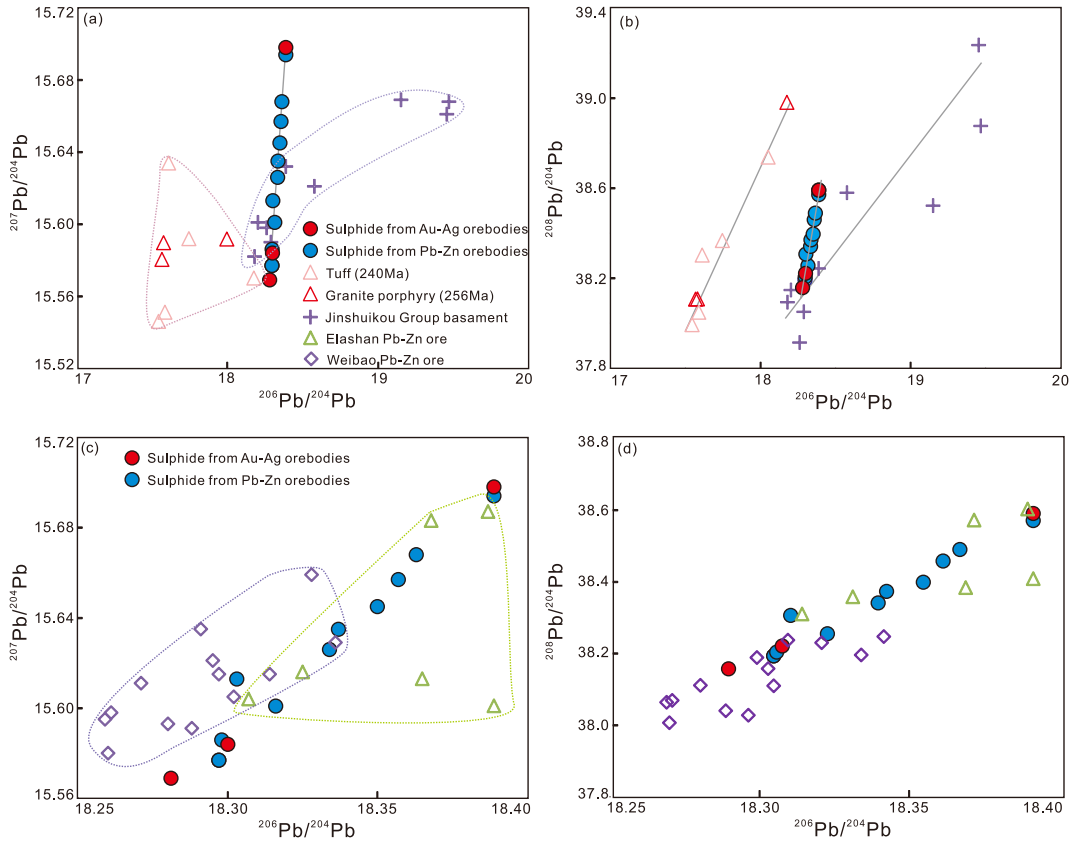

Fig. 13. Lead isotope compositions of the Kengdenongshe polymetallic deposit compared with related lithologies (a-b), and others Pb-Zn deposit in the EKO (c-d). Part of the data is from He (2013) and Jiang (2014). The lead isotope compositions of the basement are from Chen et al. (2011), the Weibo Pb-Zn ore are from Fang et al. (2015), the Elashan Pb-Zn ore are from Zhou (2015).

Table 5
Noble gas isotopic compositions of fluid inclusions hosted in pyrite from the Pb-Zn and Au-Ag rich ore bodies in the KDNS deposit.

Sample No	Mineral	Ore bodies	$^{4}He(10^{-7}$ ccSTP/g)	$^{40}Ar(10^{-7}$ccSTp/g)	$^{3}He/^{4}He$ (Ra)	$^{40}Ar/^{36}Ar$
B0806-26–1	Pyrite	Pb-Zn rich	30.741	4.095	0.03 ± 0.01	297.0 ± 2.1
B0806-26–3	Pyrite	Pb-Zn rich	72.042	4.207	0.04 ± 0.01	330.0 ± 2.4
B0810-1	Pyrite	Pb-Zn rich	101.392	3.824	0.02 ± 0.01	420.7 ± 4.7
B0812-1	Pyrite	Pb-Zn rich	15.915	1.688	0.06 ± 0.01	1011.7 ± 15.2
B3302-5–2	Pyrite	Au-Ag rich	15.630	5.139	0.07 ± 0.01	318.2 ± 3.0
B3302-8–1	Pyrite	Au-Ag rich	17.827	1.858	0.06 ± 0.01	347.5 ± 9.6

regional basement (Fig. 13a, b). The Kengdenongshe polymetallic deposit shows similar lead isotope compositions as the regional Elashan Pb-Zn and Weibao Pb-Zn-Cu ore deposit, (Fig. 13c, d). This indicates that the metals for the Kengdenongshe, Elashan, and Weibao deposits were derived from the same source, i.e. a magmatic and an old basement source (Fang et al., 2015; Zhou, 2015).

6.3. Formation and modification of the Kengdenongshe Au-Ag-Pb-Zn deposit

The regional geology, mineralogy, and geochemistry of the Kengdenongshe Au-Ag-Pb-Zn ore deposit (Table 6), suggest that it can be classified as a type VMS ore deposit. This is based on the following: (1) Silicious volcaniclastic rocks-hosted VMS deposits generated in back-arc basins are enriched in Au and Ag but relatively depleted of Cu (Barrie and Hannington, 1999; Franklin et al., 2005; Herrington et al., 2005). This applies to the Kengdenongshe polymetallic deposit, as both of the Pb-Zn rich and Au-Ag rich ore bodies in the Kengdenongshe are closely associated with the Late Permian to Triassic marine rhyolitic tuff (Wang, 2017; Xia, 2017), which relates to the transition from back-arc extension to continental collision in the EKO (Zhao et al., 2020). (2) For the Kengdenongshe deposit, although the Au + Ag-barite zone underlies the Pb-Zn zone (Fig. 4), which is different from the typical VMS model in which that Au-Ag-barite zone overlies the Pb-Zn zone (Barrie and Hannington 1999), this discrepancy is the result from later tectonic displacement. In the Middle to Late Triassic, the EKO is characterized by NS compressive stress driven by the arc-continent collision (Yin and Zhang, 1997; Li, 2012), which causes deformation of regional strata (Li, 2012). In the Kengdenongshe, the folds of Carboniferous carbonate rocks and Late Permian to Middle Triassic rhyolitic tuff is observed in filed investigation and the reverse of the ore-hosted rhyolitic tuff is further suggested by the ages of the tuff in different locations. Our drill core samples yield a concordant age of 240 Ma (Zhao et al., 2020), which is similar to the age given by Xia (2017) of 243 Ma, but younger than the age of 262 Ma from an outcrop sample (Wang, 2017). (3) The alteration assemblages in the Kengdenongshe polymetallic deposit, including quartz + chlorite + epidote, quartz + K-feldspar, and quartz + barite + marble, are typical for VMS deposits (e.g., Mills et al., 2016; Patten et al., 2016). (4) Magmatic water and seawater are the main fluid sources although small amounts of meteoric water participated in the formation of the Au-Ag rich orebodies. Sulphur and lead isotopic data suggest that the Pb-Zn rich and Au-Ag rich ore bodies share the same sulfur and metal sources, which relate to both magmatism and seawater. The magmatic and marine sources of ore-forming fluids and materials are according

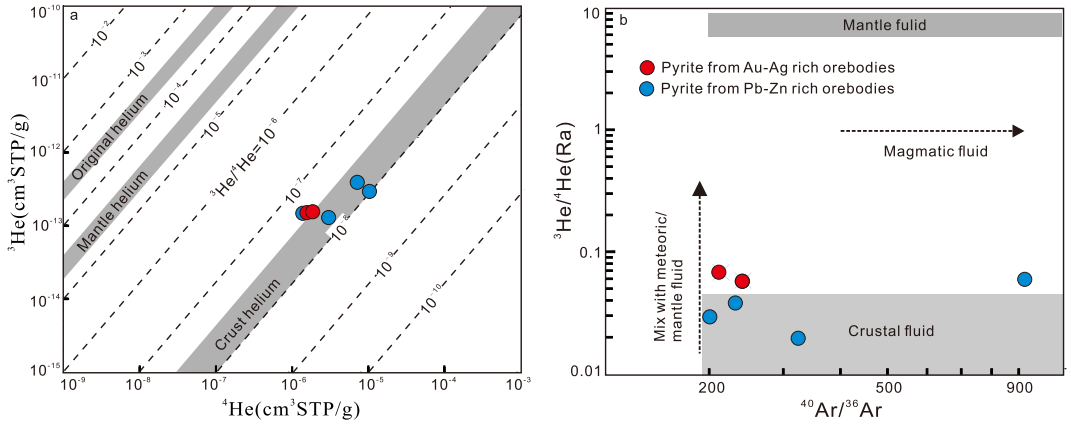

Fig. 14. He-Ar isotope compositions of fluid inclusions in pyrite from the Kengdenongshe polymetallic deposit.

Table 6
The comparision between the Pb-Zn and Au-Ag rich orebodies.

Orebodies type	Pb-Zn rich orebodies	Au-Ag rich orebodies
Location	Within the tuff (on the top of the Au-Ag rich orebodies)	Within the tuff or in the faluts connected the tuff and carbonatite
Mineral assemblage	Q + Py + Gn + Sp + Cp	Bar + Q + Py + Gn + Sp + Te + Covauriferous, argentiferous minerals
Alteration	Quartz + chlorite + epidote	Quartz + barite + marble
Metal grades (Pb, Zn wt.%; Au, Ag g/t)	Pb, 0.90; Zn, 2.77; Au 0.20; Ag, 5.65	Au, 3.67; Ag, 52.78; Pb, 0.52; Zn 0.65
Fluid source	Magmatic fluids + seawater	Magmatic fluids + seawater + meteoric water
Sulfur Source	Mgmatic derivation + seawater	Mgmatic derivation + seawater
Metals Source	Mgmatism + old crustal basement	Mgmatism + old crustal basement
Generation	Felsic clastic rocks hosted VMS type mineralization in back-arc basin	

The abbreviations, Q:quartz; Cp: chalcopyrite; Gn: galena; Sph: sphalerite; Py: pyrite; Te: tetrahedrite; Cov: covellite.

with the conditions of a VMS deposit (e.g. Dubé et al., 2007; Gill et al., 2019).

The pyrites in the Au-Ag rich ore bodies nearby the faults can be subdivided into earlier strawberry pyrite and later euhedral to subhedral pyrite. The earlier strawberry pyrite is consistent with a Late Permian to Early Triassic marine back arc setting in back-arc basin (Xia, 2017). The eu- to subhedral pyrite veins, which contain tuff breccia (Fig. 6e, f), suggest that late hydrothermal activity coincided with the deformation of the tuff and ore bodies. The meteoric water contribution to the formation of the Au-Ag rich ore bodies also supports later hydrothermal activity. However, the Au-Ag-barite orebodies have the same sulfur and metal sources as the Pb-Zn orebodies, which are all associated with the marine volcanic activity in a back-arc basin, suggesting that the Au-Ag and Pb-Zn mineralization are part of the same VMS-type mineralization event in a back-arc basin environment (Fig. 15a). later structural modification and hydrothermal activity mainly change the locations of the orebodies (Fig. 15b).

In summary, during Late Permian to Early Triassic back-arc extension in the EKO (Zhao et al., 2019, 2020), marine volcanic processes resulted in the formation of Late Permian to Triassic tuff. The magmatic water carried metallogenic materials that mixed with seawater and extracted crustal metals during ascent, and generated the VMS-type Au-Ag-Pb-Zn Kengdenongshe ore deposit (Fig. 15a). Middle to Late Triassic continental collision in the EKO caused displacement of the Au-Ag and Pb-Zn rich ore bodies (Fig. 15b).

7. Conclusions

(1) Ore bodies in the Kengdenongshe polymetallic deposit can be subdivided into Au-Ag rich orebodies and Pb-Zn rich orebodies. There are contributions of magmatic water and seawater to both type ore bodies and additional involvement of meteoric water in the Au-Ag rich ore bodies. The Au-Ag and Pb-Zn rich ore bodies share the same sulfur and lead sources. The sulfur has a crustal magmatic and a seawater sulfate source while the lead has a magmatic and an old crustal sedimentary source.

(2) The Kengdenongshe polymetallic deposit can be categorised as a VMS-type. Deposit. Both the mineralization of Au-Ag and Pb-Zn and the formation of ore-hosted tuff occurred as a result of marine volcanic processes in a Late Permian to Early Triassic back-arc extensional environment.

(3) The structural activities driven by are-continent collision in Triassic caused the displacement of the location of Au-Ag and Pb-Zn rich ore bodies.

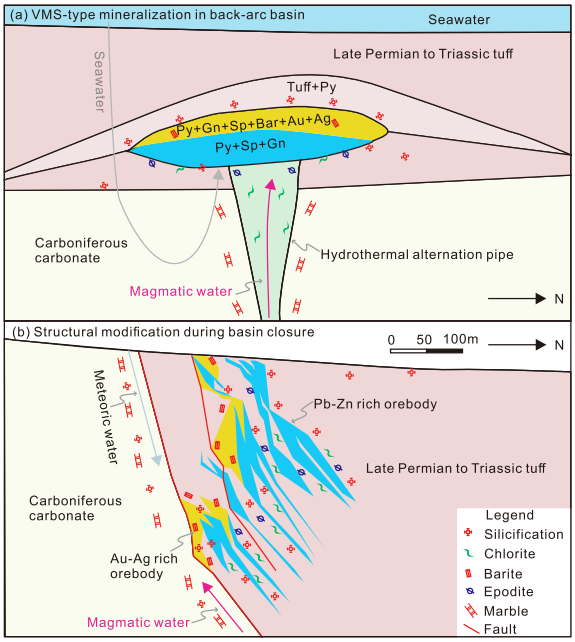

Fig. 15. Cartoons show the generation and modification of the Kengdenongshe polymetallic deposit. Cp: chalcopyrite; Gn: galena; Sph: sphalerite; Py: pyrite; Bar: barite.

Declaration of Competing Interest

The authors declare that they have no known competing financial interests or personal relationships that could have appeared to influence the work reported in this paper.

Acknowledgements

This study is supported by the National Natural Science Foundation of China (41972086), and the China Geological Survey (12120114081401, 12120114000701). We would like to thank the editor-in-chief Franco Pirajno for handling our manuscript. We are grateful for the kind suggestions and comments from the two anonymous reviewers. We would also like to thank the valuable help from Yujing Zhao, Yang Tang, and Junlin Chen from the China University of Geosciences during field work.

References

Allen, R.L., Weihed, P., the Global VHMS Research Project team, 2002. Global comparison of volcanic-associated massive sulphide districts. In: Blundell, D.J., Neubauer, F., von Quadt, A. (Eds.), The Timing and Location of Major Ore Deposits in an Evolving Orogen. Geological Society, London, Special Publications no. 204, pp. 13–37.

Anderson, I.K., Ashton, J.H., Boyce, A.J., Fallick, A.E., Russell, M.J., 1998. Ore depositional processes in the Navan Zn+Pb deposit, Ireland. Econ. Geol. 93, 535–563.

Barrie, C.T., Hannington, M.D., 1999. Volcanic Associated massive sulfide deposits: Processes and examples in modern and ancient settings. Rev. Econ. Geol. 8, 74–100.

Basuki, N.I., Taylor, B.E., Spooner, E.T.C., 2008. Sulfur isotope evidence for thermochemical reduction of dissolved sulfate in Mississippi Valley-tye zinc-lead mineralization, Bongara area, northern Peru. Econ. Geol. 103 (4), 783–799.

Brown, P.E., Hagemann, S.G., 1995. MacFlinCor and its application to fluids in Archean lode-gold deposits. Geochim. Cosmochim. Acta 59 (19), 3943–3952.

Burnard, P.G., Hu, R., Turner, G., Bi, X.W., 1999. Mantle, crustal and atmospheric noble gases in Ailaoshan Gold deposits, Yunnan Province, China. Geochim. Cosmochim. Acta 63, 1595–1604.

Chen, J., Wang, H.N., 2004. Geochemistry. Science Press, Beijing.

Chen, J.J. 2018. Paleozoic-Mesozoic tectono-magmatic evolution and gold mineralization in Gouli Area, east end of East Kunlun Orogen. China University of Geosciences, pp. 1-222 (in Chinese with English abstract).

Chen, J.J., Fu, L.B., Wei, J.H., Tian, N., Xiong, L., Zhao, Y.J., Zhang, Y.J., Qi, Y.Q., 2016. Geochemical characteristics of the Late Ordovician granodiorite in the Gouli area, Eastern Kunlun Orogenic Belt, Qinghai Province: Implications on the evolution of the Proto-Tethys Ocean. Earth Sci. J. China Univ. Geosci. 41 (11), 1863–1882 (in Chinese with English abstract).

Chen, J.J., Wei, J.H., Fu, L.B., Li, H., Zhou, H.H., Zhao, X., Zhan, X.F., Tan, J., 2017. Multiple sources of the early Mesozoic Gouli batholith, eastern Kunlun Orogenic Belt, northern Tibetan plateau: linking continental crustal growth with oceanic subduction. Lithos 292–293, 161–178.

Chen, L., Sun, Y., Pei, X.Z., Feng, T., Zhang, G.W., 2004. Comparison of eastern paleo-Tethyan ophiolites and its geodynamic significance——Evidence from Dur'ngoi ophiolite. Sci. China Earth Sci. 47 (4), 378–384 (in Chinese with English abstract).

Chen, N.S., Li, X.Y., Zhang, K.X., Wang, G.C., Zhu, Y.H., Hou, G.J., Bai, Y.S., 2006. Lithological characteristics of the Baishahe formation to the south of Xiangride Town, Eastern Kunlun Mountains and its age constrained from zircon Pb-Pb dating. Geol. Sci. Technol. Inf. 25 (6), 1–7 (in Chinese with English abstract).

Chen, X.H., Yin, A., George, G., Li, L., Jiang, R.B., 2011. Chemical geodynamics of granitic magmatism in the basement of the eastern Qaidam basin, northern Qinghai-Tibet Plateau. Acta Geol. Sin. 85, 157–171.

Chen, Y.X., Pei, X.Z., Li, R.B., Li, Z.C., Pei, L., Chen, G.C., Liu, C.J., Li, X.B., Yang, J., 2013. Zircon U-Pb age,geochemical characteristics and tectonic significance of metavolcanic rocks from Naij Tal Group, east section of East Kunlun. Earth Sci. Front. 20 (6), 240–254 (in Chinese with English abstract).

Chiaradia, M., Tripodi, D., Fontboté, L., Reza, B., 2008. Geologic setting, mineralogy, and geochemistry of the Early Tertiary Au-rich volcanic-hosted massive sulfide deposit of La Plata, Western Cordillera, Ecuador. Econ. Geol. 103, 161–183.

Clayton, R.N., Mayeda, T.K., 1963. The use of bromine penta-fluoride in the extraction of oxygen from oxides and silicates for isotopic analysis. Geochim. Cosmochim. Acta 27, 43–52.

Clayton, R.N., O'Neil, J.R., Mayeda, T.K., 1972. Oxygen isotope exchange between quartz and water. J. Geophys. Res. 7, 3055–3067.

Dixon, G., Davidson, G.J., 1996. Stable isotope evidence for thermochemical sulfate reduction in the Dugald river (Australia)strata-bound shale-hosted zinc-lead deposit. Chem. Geol. 129 (3–4), 227–246.

Dubé, B., Langevin, P.M., Hannington, M.D., Lafrance, B., Gosselin, G., Gosselin, P., 2007. The LaRonde Penna world-class Au-rich volcanogenic massive sulfide deposit, Abitibi, Québec: Mineralogy and geochemistry of alteration and implications for genesis and exploration. Econ. Geol. 102 (4), 633–666.

Emsbo, P., Hutchinson, R.W., Hofstra, A.H., Volk, J.A., Bettles, K.H., Baschuk, G.J., Johnson, C.A., 1999. Syngenetic Au on the Carlin trend: Implications for Carlin-type deposits. Geology 27 (1), 59–62.

Fang, J., Chen, H.Y., Zhang, L., Zheng, Y., Li, D.F., Wang, C.M., Shen, D.L., 2015. Ore genesis of the Weibao lead–zinc district, Eastern Kunlun Orogen, China: constrains from ore geology, fluid inclusion and isotope geochemistry. Int. J. Earth Sci. 104 (5), 1209–1233.

Franklin, J.M., Gibson, H.L., Jonasson, I.R., Galley, A.G., 2005. Volcanogenic massive sulfide deposits. Econ. Geol. 100th Anniv. 98, 523–560.

Gao, X.F., Xiao, P.X., Xie, C.R., Fan, L.Y., Guo, L., Xi, R.G., 2010. Zircon LA-ICP-MS U-Pb dating and geological significance of Bashierxi granite in the eastern Kunlun area, China. Geol. Bull. China 29 (7), 1001–1008 (in Chinese with English abstract).

Gibson, H., Franklin, J.M., Hannington, M.D., 2000. A genetic model for volcanic-associated massive sulfide deposits, an overview of progress made and problems remaining. GeoCanada 2000—The Millennium Geoscience Summit, Conference Abstract, vol. 758. 4 pp.

Gill, S.B., Piercey, S.J., Layne, G.D., Piercey, G., 2019. Sulphur and lead isotope geochemistry of sulphide minerals from the Zn-Pb-Cu-Ag-Au Lemarchant volcanogenic massive sulphide (VMS) deposit, Newfoundland, Canada. Ore Geol. Rev. 104, 422–435.

Guo, C.L., Dong, Z.C., Li, Y., Niu, F.Y., 2013. Study on the occurrence of gold and silver in Qinghai Kangdenongshe polymetallic deposit. Gold 3 (34), 28–30 (in Chinese with English abstract).

He, C.F., 2013. The Metllogenic Geological Characteristics Kangdenongshe Barite Type Gold-Polymetallic Deposit. Qinghai. China University of Geosciences (Beijing) 1–44 (in Chinese with English abstract).

He, D.F., Dong, Y.P., Liu, X.M., Yang, Z., Sun, S.S., Cheng, B., Li, W., 2016. Tectono-thermal events in East Kunlun, Northern Tibetan Plateau: Evidence from zircon U-Pb geochronology. Gondwana Res. 30, 179–190.

Herrington, R., Maslennikov, V., Zaykov, V., Seravkin, I., Kosarev, A., Buschmann, B., Orgeval, J.-J., Holland, N., Tesalina, S., Nimis, P., Armstrong, R., 2005. Classification of VMS deposits: lessons from the South Uralides. Ore Geol. Rev. 27 (1–4), 203–237.

Herzig, P.M., Hannington, M.D., 1995. Polymetallic massive sulfide at the modern seafloor: a review. Ore Geol. Rev. 10 (2), 95–115.

Hou, Z.Q., Khin, Z., Qu, X.M., Ye, Q.T., Yu, J.J., 2001. Origin of the Gacun volcanic-hosted massive sulfide deposit in Sichuan, China: Fluid inclusion and oxygen isotope evidence. Econ. Geol. 96 (7), 1491–1512.

Jiang, M.G., 2014. Genesis and metallogenic regularity of Kengdenongshe Au-Pb-Zn polymetallic deposit, Maduo county. Qinghai Province. Central South University 1–105 (in Chinese with English abstract).

Jin, L.J., Zhou, H.W., Zhu, Y.H., Lin, Q.X., 2015. U-Pb age of the detrital zircon from the serteng formation in East Kunlun: Constraints on its provenance and formation time. Geotectonica et Metallogenia 39 (4), 691–703 (in Chinese with English abstract).

Ke, L.L., Zhang, H.Y., Liu, J.J., Zhai, D.G., Guo, D.H., Yang, J.K., Tan, Q., Xu, Y.W., Zhang, M., Wang, S.G., 2017. Fluid Inclusion, H-O, S, Pb and noble gas isotope studies of the Aerhada Pb-Zn-Ag deposit, Inner Mongolia, NE China. Ore Geol. Rev. 88, 304–316.

Lafrance, B., Davis, D.W., Goutier, J., Moorhead, J., Pilote, P., Mercier-Langevin, P., Dubé, B., Galley, A.G., and Mueller, W.U., 2005, Nouvelles datations isotopiques dans la portion québécoise du Groupe de Blake River et des unités adjacentes : Ministère des Ressources naturelles, de la Faune et des Parcs du Québec, RP 2005-01, 15 p.

Langevin, P.M., Dubé, B., Hannington, M.D., Davis, D.W., Lafrance, B., Gosselin, G., 2007. The LaRonde Penna Au-rich volcanogenic massive sulfide deposit, Abitibi greenstone belt, Quebec: Part I Geology and Geochronology. Econ. Geol. 102 (4), 585–609.

Li, R.B., 2012. Research on the Late Paleozoic-Early Mesozoic orogeny in East Kunlun Orogen. (Doctor). Chang'an University, pp. 1–185 (in Chinese with English abstract).

Li, S., Tu, G.L., Ye, H.N., Zhao, Z.Q., 2016. Research on the process mineralogy of V1 gold polymetallic ore of Qinghai Kangdenongshe ore. J. East China Univ. Technol. Nat. Sci. 39 (4), 325–330 (in Chinese with English abstract).

Liu, Y., Fu, L.B., Wang, F.L., Wei, J.H., Guan, B., Ta, J., Wang, D.Z., 2018. Relationship between Pb-Zn and Au-Ag mineralization of Kengdenongshe polymetallic deposit in eastern segment of the Eastern Kunlun. Geotectonica et Metallogenia 42 (3), 481–493 (in Chinese with English abstract).

Liu, Z.Q., Pei, X.Z., Li, R.B., Li, Z.C., Zhang, X.F., Liu, Z.G., Chen, G.C., Chen, Y.X., Ding, S.P., Guo, J.F., 2011. LA-ICP-MS Zircon U-Pb geochronology of the two suites of ophiolites at the Buqingshan area of the A'nyemaqen orogenic belt in the southern margin of East Kunlun and its tectonic implication. Acta Geol. Sin. 30 (8), 1182–1195 (in Chinese with English abstract).

Ma, C.Q., Xiong, F.H., Yin, S., Wang, L.X., Gao, K., 2015. Intensity and cyclicity of orogenic magmatism: An example from a Paleo-Tethyan granitoid batholith, Eastern Kunlun, northern Qinghai-Tibetan Plateau. Acta Petrologica Sinica 31 (12), 3555–3568 (in Chinese with English abstract).

Mamyrin, B.A., Tolstikhin, I.N., 1984. In: Helium Isotopes in Nature. Elsevier, Amsterdam, pp. 1–267.

Matsuda, J., Matsumoto, T., Sumino, H., Nagao, K., Yamamoto, J., Miura, Y., 2002. The 3He/4He ratio of the new internal He Standard of Japan (HESJ). Geochem. J. 36, 191–195.

McNicoll, V., Dubé, B., Goutier, J., Mercier-Langevin P, Dion, C., Monecke, T., Ross, P.S., Thurston, P., Percival, J., Legault, M., Pilote, P., Bédard, J., Leclerc, F., Gibson, H., Ayer, J., 2008. New U-Pb geochronology from the TGI-3 Abitibi/Plan Cuivre project: implications for geological interpretations and base metal exploration. Geological Association of Canada – Mineralogical Association of Canada (GAC-MAC-SEG-SGA) Joint Annual Meeting, Quebec City, May 2008, Abstracts Volume 33, p. 110.

Mercier-Langevin, P., Hannington, M.D., Dubé, B., Bécu, V., 2011. The gold content of volcanogenic massive sulfide deposits. Miner. Deposita 46 (5–6), 509–539.
Mills, H.K., Piercey, S.J., Toole, T., 2016. Geology, alteration, and lithogeochemistry of the Hood volcanogenic massive sulfide (VMS) deposits, Nunavut, Canada. . Mineralium Deposita 51 (4), 533–556.
Misra, K., 2000. In: Understanding Mineral Deposits. Kluwer Academic Publishing House, London, p. 845.
Mo, X.X., Luo, Z.H., Deng, J.F., Yu, X.H., Liu, C.D., Shen, H.W., Yuan, W.M., Luo, Z.H., 2007. Granitoids and crustal growth in the East-Kunlun orogenic belt. Geol. J. China Univ. 13 (3), 403–414 (in Chinese with English abstract).
Ohmoto, H., 1972. Systematics of sulfur and carbon isotopes in hydrothermal ore deposits. Econ. Geol. 67, 551–578.
Ohmoto, H., Rye, R.O., 1979. Isotopes of sulfur and carbon. In: Barnes, H.L. (Ed.), Geochemistry of Hydrothermal Ore Deposit. Wiley, New York, pp. 509–567.
Ouyang, H.G., Mao, J.W., Santosh, M., Wu, Y., Hou, L., Wang, X.F., 2014. The Early Cretaceous Weilasituo Zn–Cu–Ag vein deposit in the southern Great Xing'an Range, northeast China: Fluid inclusions, H, O, S, Pb isotope geochemistry and genetic implications. Ore Geol. Rev. 56, 503–515.
Ozima, M., Podosek, F.A., 2002. In: Noble Gas Geochemistry. Cambridge University Press, Cambridge, pp. 1–286.
Patten, C.G., Pitcairn, I.K., Teagle, D.A., Harris, M., 2016. Mobility of Au and related elements during the hydrothermal alteration of the oceanic crust: implications for the sources of metals in VMS deposits. Miner. Deposita 51 (2), 179–200.
Stuart, F.M., Burnard, P.G., Taylor, R.P., Turner, G., 1995. Resolving mantle and crustal contributions to ancient hydrothermal fluids: He-Ar isotopes in fluid inclusions from Dae Hwa W-Mo mineralisation, South Korea. Geochim. Cosmochim. Acta 59, 4663–4673.
Tang, Y., Bi, X.W., Fayek, M., Stuart, F.M., Wu, L.Y., Jiang, G.H., Xu, L.L., Liang, F., 2017. Genesis of the Jinding Zn-Pb deposit, northwest Yunnan Province, China: Constraints from rare earth elements and noble gas isotopes. Ore Geol. Rev. 90, 970–986.
Tomkins, A.G., 2007. Three mechanisms of ore re-mobilisation during amphibolite facies metamorphism at the Montauban Zn–Pb–Au–Ag deposit. Miner. Deposita 42 (6), 627–637.
Wang, C.H., 2017. Geology and geochemistry of Kengdenongshe gold and polymetallic deposit in Maduo, Qinghai. China Univ. Geosci. Beijing 1–114 (in Chinese with English abstract).
Wang, G.C., Wang, Q.H., Jian, P., Zhu, Y.H., 2004. Zircon SHRIMP ages of Precambrian metamorphic basement rocks and their tectonic significance in the eastern Kunlun Mountains, Qinghai Province, China. Earth Sci. Front. 11 (4), 481–490 (in Chinese with English abstract).
Wang, G.C., Wei, Q.R., Jia, C.X., Zhang, K.X., Li, D.W., Zhu, Y.H., Xiang, S.Y., 2007. Some ideas of Precambrian geology in the East Kunlun, China. Geol. Bull. China 26 (8), 929–937 (in Chinese with English abstract).
Xia, R., 2017. Paleo-tethys orogenic process and gold metallogenesis of the East Kunlun. China Univ. Geosci. Beijing 1–215 (in Chinese with English abstract).
Xiong, F.H., Ma, C.Q., Zhang, J.Y., Liu, B., Jiang, H.A., 2014. Reworking of old continental lithosphere: an important crustal evolution mechanism in orogenic belts, as evidenced by Triassic I-type granitoids in the East Kunlun orogen, Northern Tibetan Plateau. J. Geol. Soc. 171, 847–863.
Xu, Z.Q., Dilek, Y., Cao, H., Yang, J.S., Robinson, P., Ma, C.Q., Li, H.Q., Jolivet, M., Roger, F., Chen, X.J., 2015. Paleo-Tethyan evolution of Tibet as recorded in the East Cimmerides and West Cathaysides. J. Asian Earth Sci. 105, 320–337.
Xu, Z.Q., Li, H.B., 2006. An orogenic plateau—The orogenic collage and orogenic types of the Qinghai-Tibet plateau. Earth Sci. Front. 13 (4), 1–17 (In Chinese with English abstract).
Yang, J.S., Robinson, P.T., Jiang, C.F., Xu, Z.Q., 1996. Ophiolites of the Kunlun Mountains, China and their tectonic implications. Tectonophysics 258 (1–4), 215–231.
Yin, H.F., Zhang, K.X., 1997. Characteristics of the East Kunlun orogenic belt. Earth Sci. J. China Univ. Geosci. 22 (4), 3–6 (in Chinese and English abstract).
Zhang, D.Q., Dang, X.Y., She, H.Q., Li, D.X., Feng, C.Y., Li, J.W., 2005. Ar-Ar dating of orogenic gold deposits in northern margin of Qaidam and East Kunlun Mountains and its geological significance. Mineral Deposits 24, 87–98 (in Chinese with English abstract).
Zhang, J., Ma, C., Xiong, F., Liu, B., Li, J., Pan, Y., 2014. Early Paleozoic high-Mg diorite-granodiorite in the eastern Kunlun Orogen, western China: Response to continental collision and slab break-off. Lithos 210–211, 129–146.
Zhao, X., Fu, L.B., Wei, J.H., Bagas, L., Santosh, M., Liu, Y., Zhang, D.H., Zhou, H.Z., 2019. Late Permian back-arc extension of the eastern Paleo-Tethys Ocean: Evidence from the East Kunlun Orogen, northern Tibetan Plateau. Lithos 340–341, 34–48.
Zhao, X., Fu, L.B., Wei, J.H., Zhao, Y.J., Tang, Y., Yang, B.R., Guan, B., Wang, X.Y., 2018. Geochemical characteristics of the An'nage hornblende gabbro from East Kunlun Orogenic Belt: Constraints on the evolution of Paleo-Tethys Ocean. Earth Sci. J. China Univ. Geosci. 43 (2), 354–370 (in Chinese with English abstract).
Zhao, X., Wei, J., Fu, L., Huizenga, J.M., Santosh, M., Chen, J.J., Wang, D.J., Li, A.B., 2020. Multi-stage crustal melting from Late Permian back-arc extension through Middle Triassic continental collision to Late Triassic post-collisional extension in the East Kunlun Orogen. Lithos 105446.
Zhou, H.H., 2015. Metallogenic prediction and the controlling role of volcanic and sub-volcanic rocks for mineralization in the Elashankou copper polymetallic deposit, Qinghai Province. China Univ. Geosci. 1–126 (in Chinese with English abstract).